Automated profile analysis for single-crystal diffraction data

R. J. Angel

Automated profile analysis for single-crystal diffraction data

R. J. Angel

Crystallography Laboratory, Dept. Geological Sciences, Virginia Tech, Blacksburg, VA 24060, USA. Correspondence e-mail: rangel@vt.edu

An integration method for step-scanned single-crystal intensity data based upon fitting of the individual diffraction profiles by a pseudo-Voigt function is presented. Algorithms for both the recovery of weak intensities from data sets and the rejection of aberrant peak profiles are discussed. The ideas presented in this paper have been implemented in a software package for Microsoft Windows, *WinIntegrStp*, which is available at http://www.crystal.vt.edu/.

1. Introduction

Changes in crystal structure with temperature or pressure are generally subtle. Therefore the most accurate intensity data are required in order to follow reliably the evolution of structures with pressure or temperature through a series of structure refinements using intensity data collected at different conditions. Yet high-pressure intensity data, in particular, are of intrinsically lower quality than data collected in air. Diffracted intensities are reduced by absorption by the components of the pressure cell, while scattering from the latter leads to high levels of highly structured background intensity. Furthermore, access to the sample is restricted. This has two important consequences. First, the total number of accessible reflections is typically one-third or less of the entire data set (*e.g.* Finger & King, 1978). A few incorrect integrated intensities can therefore strongly bias a structure refinement, resulting in incorrect values of positional and thermal parameters. Second, the collection of symmetry-equivalent reflections is limited and the identification and rejection of aberrant intensities by averaging symmetry-equivalent reflections (*e.g.* Blessing, 1987) is often not possible. Although new data collection procedures have been developed to reduce and/or identify incorrect intensities (*e.g.* Angel *et al.*, 2000; Loveday *et al.*, 1990) the ability to obtain an accurate structure refinement from high-pressure diffraction data remains critically dependent on the recovery of the maximum possible number of accurate intensities from the data set and the exclusion of incorrect intensity data.

It has long been acknowledged that the collection of single-crystal intensity data by step scans offers considerable advantages over alternative methods that integrate the diffracted intensity either in the detector itself or its associated electronics (*e.g.* Diamond, 1969; Blessing *et al.*, 1974; Pavese & Artioli, 1996). The storage of step-scanned data offers the opportunity to identify double diffraction events and interference from environmental cells, as well as allowing corrections to be made for such effects as non-uniform backgrounds and thermal diffuse scattering. Yet most available software do not exploit this potential of step-scanned data and instead employs what might be termed the 'traditional' or 'counting' method of integration, often called 'background–peak–background'. A certain percentage of both ends of each scan are pre-defined as background, and the counts at the steps between these limits are assigned to the integrated intensity of the peak from which the background is subsequently subtracted. Some integration programs implement a dynamic setting of the background limits, often following the algorithm proposed by Lehmann & Larsen (1974). This algorithm has the advantage over fixed background methods that it improves the $I/$e.s.d.(I) ratio by only integrating the peak area. The dynamic setting of background limits also allows for the peak being slightly offset from the middle of the scan range. However, while these 'counting' methods for the integration of step scans provide good estimates of integrated intensities for peaks with good signal-to-noise ratios, they have several limitations. They provide no information about peak shape with which to test whether the maximum in a step scan actually arises from the crystal diffraction, or whether it is an artefact, perhaps arising from diffraction from an environmental cell. Neither do 'counting' methods provide a mechanism for the recovery of weak reflections from data sets. As a consequence, experience has shown that in order to obtain high-quality structure refinements from crystals held at high pressures in diamond-anvil cells, every reflection profile in a data set must be visually examined by the experimentalist, which is a long and tedious process open to human misjudgement and error.

By contrast, 'learnt-profile' (Diamond, 1969; Gałdecka, 1999) and peak-profiling methods in which the step-scan data for each reflection are fitted with an appropriate profile function provide the possibility of addressing these issues (Pavese & Artioli, 1996). Tests for peak rejection can be quantified, based on the refined peak shape parameters. The parameters for the profile functions and the positions of the weaker peaks can be constrained from the more reliable values obtained from refinement to the stronger peaks. More weak intensities can thereby be recovered from the data set. Together, these two properties of peak profiling allow the

entire integration process to be automated. For a full historical review of peak-profiling methods as applied to single-crystal diffraction data, the reader is encouraged to consult the work of Pavese & Artioli (1996) and the references therein. In this paper a practical implementation of peak-profiling methods based upon the work of Pavese & Artioli (1996) is described.

2. Methods

2.1. Profile function

Following Gałdecka (1993) and Pavese & Artioli (1996), an ω step scan over a diffraction maxima can be described as a pair of pseudo-Voigt functions representing the α_1 and α_2 contributions to the profile, plus a locally constant background term

$$I(\omega) = \mathrm{PV}_1(\omega) + \mathrm{PV}_2(\omega) + \mathrm{constant}. \tag{1}$$

Each single pseudo-Voigt function is written as

$$\mathrm{PV}(\omega) = \frac{I\eta\Gamma}{2\pi(\omega - \omega_0)^2 + \Gamma^2} + \frac{2I(1-\eta)(\ln 2)^{1/2}}{\Gamma\pi^{1/2}}$$
$$\times \exp\left\{-\left[\frac{2(\omega - \omega_0)(\ln 2)^{1/2}}{\Gamma}\right]^2\right\}. \tag{2}$$

The four refineable parameters for a single pseudo-Voigt function are thus position ω_0, total integrated intensity I, the full width of the peak at half-maximum Γ, and the mixing parameter η, which is zero for a pure Gaussian peak and 1 for a pure Lorentzian. The numerical constants π and $(\ln 2)^{1/2}$ in (2) serve to normalize the profile so that the parameter I is the true integrated intensity proportional to $|F_{\mathrm{obs}}^2|$ after correction for geometric and polarization factors. Asymmetry of the peak profile could be included (e.g. Gałdecka, 1993) but has not yet been found to be necessary in practice for data sets collected with laboratory diffractometers.

When both α_1 and α_2 wavelengths contribute peaks to the profile [as in equation (1)] it is reasonable to assume that both peaks have the same η and Γ parameters. The position of the α_2 peak is calculated from that of the α_1 peak plus an offset due to the known α_1/α_2 dispersion (see below). The relative integrated intensity of the α_2 peak is expressed in terms of a refineable parameter $I_{\mathrm{ratio}} = I(\alpha_2)/I(\alpha_1)$. The peak function defined by equations (1) and (2) then provides a reasonable representation of the peak shape over a wide range of Bragg angles. This formulation therefore results in six refineable parameters for each reflection scan: the background term, the full width of the both peaks at half-maximum Γ, the integrated intensity of the α_1 peak, the position ω_0 of the α_1 peak, the mixing parameter η of both peaks, and the intensity of the α_2 peak as a fraction of the α_1 peak, $I_{\mathrm{ratio}} = I(\alpha_2)/I(\alpha_1)$.

The offset of the position of the α_2 peak from the α_1 peak is not a refineable parameter, but depends on the geometry of the incident beam optics on the diffractometer. For an unmonochromated source, and also for one with a monochromator whose diffracting plane is $90°$ from that of the diffractometer, the offset of the α_2 peak is $\arcsin(\lambda_2 \sin\theta_1/\lambda_1)$

$- \theta_1$. The frequently used approximation $\Delta\lambda/\lambda \tan\theta_1$ for this offset is in error by $\sim 10^{-4}$ degrees at $2\theta = 40°$ and by $\sim 10^{-3}$ degrees for $2\theta > 80°$ for Mo $K\alpha$ radiation. For a monochromator in parallel geometry there can be an additional offset of the α_2 peak due to the α_1–α_2 dispersion by the monochromator crystal. This additional offset is added to the sample dispersion when the detector lies on one side of the direct beam, and subtracted when the detector lies on the other side.

2.2. Peak discrimination tests

As noted above, the refinement of a peak profile function provides the opportunity to test for abnormal peak shapes automatically and to reject the corresponding intensity data. The success, or otherwise, of an implementation of an automatic method of integration depends upon its ability to discriminate against profile maxima with aberrant shapes, while retaining valid profiles and recovering integrated intensities from weak but valid data. Extensive testing has indicated that the order in which the various tests are applied to the profile parameters makes a significant difference to the success or otherwise of this discrimination process. The following sequence of tests is the one that has, so far, been
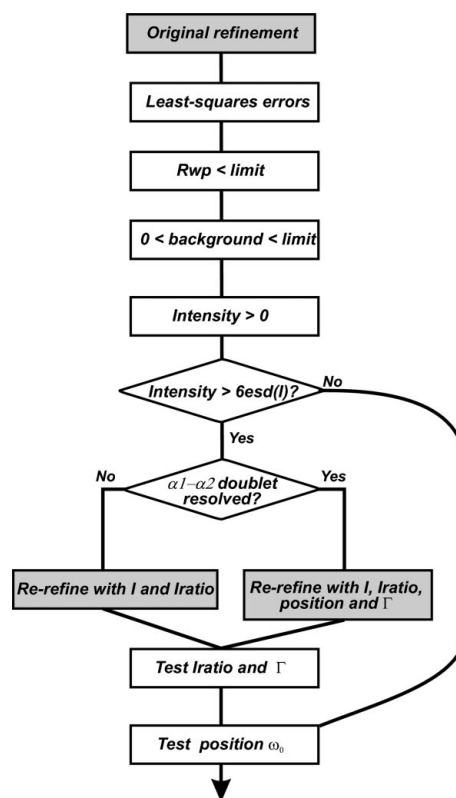

Figure 1
A flow chart illustrating the sequence of tests applied to the refined parameters of a profile function. Grey boxes indicate refinements, while white rectangular boxes indicate the tests. The test sequence is exited at the first failure. During the main integration of a data set, those reflections that fail on the first cycle of tests are re-integrated with the position of the peak function fixed by the **UB** matrix. The test sequence is then repeated on the new profile parameters.

found to be the most reliable in terms of both rejecting aberrant profiles and not rejecting valid profiles. A flow chart summarizing this sequence appears as Fig. 1.

The first group of tests is applied to all profile refinements.

(i) Least-squares errors, including non-convergence in the refinement, invalid data, and various math errors. In practice these are exceedingly rare except when the data scan does not actually contain a maximum in the count rate.

(ii) $R_{wp} = \sum w_i(y_{i,obs} - y_{i,calc})^2 / \sum w_i y_{i,obs}^2$ is tested against a preset value; twice the value of R_{wp} of the strong reflections in the data set appears to provide good discrimination. R_{wp} appears to be a more sensitive test of peak shape than alternative measures of fit. The test is not, however, applied if the reflection has unequal backgrounds at the two ends of the scan range because this case invariably leads to rejection as a result of the higher background (often a diffraction peak from a cell component) not being fitted.
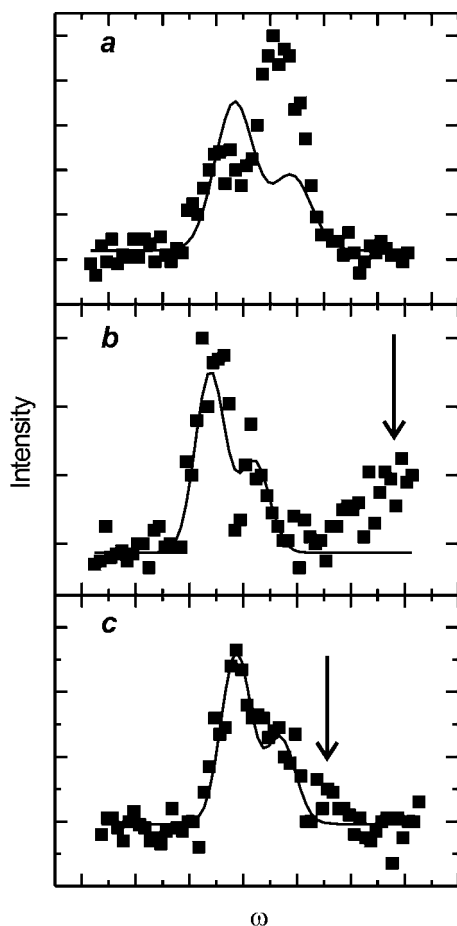

Figure 2
Observed (symbols) and fitted (line) peak profile functions. (*a*) A case of double diffraction leading to an incorrect profile and rejection by the test sequence in the fitting procedure. This peak would be integrated by a simple 'counting method'. Interference by diffraction from a diamond-cell component (arrowed) in the profiles shown in (*b*) and (*c*) is excluded by the fitting routine. 'Counting method' integration underestimates the intensity of the profile in (*b*) because of the high background at the end of the scan, but overestimates the intensity in (*c*) by including the cell contribution in the peak intensity.

(iii) Background level against preset values (usually zero for minimum and a sensibly chosen maximum value).

(iv) Intensity against a minimum preset value (usually 0).

The peak shape is then tested because this provides a good discrimination against peaks affected by double diffraction events (*e.g.* Fig. 2*a*). However, these tests involve the re-refinement of additional profile parameters and are therefore not reliable for low intensities. A cut-off of $I/\sigma(I) > 6$ appears to be reasonable.

(v) A second refinement is performed in which the intensity and I_{ratio} are refined. If the $\alpha_1-\alpha_2$ doublet is well resolved, then Γ and the peak position are also refined. The values of Γ or I_{ratio} from this re-refinement are then tested against pre-set limits.

The last test is applied to all reflections:

(vi) The deviation of the peak position ω_0 from the centre of the scan is tested against pre-set limits. This test is applied to the original refinement if $I/\sigma(I) < 6$, or to the re-refinement if $I/\sigma(I) > 6$.

The limits to what are considered valid parameter values must be chosen in the light of the quality of the individual data set, although default values can be selected that are suitable for a majority of data sets from a given instrument. The effect on the integration of a particular data set of these limiting values can be quickly explored provided that a graphical interface is part of the integration program.

3. Implementation

In order to obtain the best estimates of intensities from the integration process, it is useful to constrain some of the other five parameters in the least-squares refinement of each scan. This is particularly important for weak reflections, for which parameter correlations can lead in a full refinement to physically meaningless parameter values such as negative intensities. The underlying principle to be applied is that the shapes of the profiles of all of the reflections from one crystal on one diffractometer can be described by either constant values for the parameters (*e.g.* Diamond, 1969), or by values that vary smoothly and systematically across the data set. The first step of an integration is therefore some 'preliminary processing' of the data set to determine these values. These values are then employed in the 'main integration' of the entire data set, including the recovery of the weak reflection data. The overall procedure is based in part on the ideas developed by Pavese & Artioli (1996). In a sense this procedure is similar to the 'learnt-profile' approach (*e.g.* Diamond, 1969; Gałdecka, 1999, 2002), but here a specific profile function for each component of the doublet is being imposed *a priori* as a model.

3.1. Preliminary processing

The values of the peak-shape parameter η and the intensity ratio I_{ratio} are often found to be the same for all data sets collected with a given diffractometer configuration, indicating that the incident beam profile is dominating the peak shape. In

such cases any variation in the values of these two profile parameters becomes an extremely sensitive indicator of a change in the alignment of the diffractometer and incident-beam optics. Neither parameter can be reliably determined from low-angle reflections because the overlap of the α_1 and α_2 components leads to strong correlations in the least-squares refinement of the profile function. The parameters η and I_{ratio} are therefore best determined for a sample crystal by fitting a few slow scans of strong high-angle peaks from a good-quality crystal in which the doublet is well resolved. In the subsequent integration of data sets, the values of η and I_{ratio} are kept fixed at the predetermined values (see also Pavese & Artioli, 1996). If, however, the crystal contributes significantly to the peak shape, then the value of η can be expected to vary from sample to sample and must therefore be determined for each sample.

Many authors (*e.g.* Destro & Marsh, 1987; Pavese & Artioli, 1996; Gałdecka, 1999) have noted that the intensity is strongly correlated with the background parameter. Ways have therefore been sought to provide more reliable integrated intensities through fixing or constraining the background parameter. Because the level of the radiation background in a data set collected in air varies smoothly with the setting angles of the diffractometer, Pavese & Artioli (1996) used a polynomial function of the diffractometer setting angles to define the background value for each reflection. Gałdecka (2002) employed a polynomial function of 2θ combined with terms proportional to the direction cosines of the diffracted beam. However, data sets collected from crystals held in diamond-anvil pressure cells have a strong local variation in background levels that cannot be usefully described by any such global parameterization. Instead the idea of a 'fixed background' is borrowed from the 'counting' methods of integration. The background of each scan is fixed to the average of the counts of a selected number of steps at both ends of each individual scan, provided that the peak profile does not extend into the region defined as background. If the background levels at the two ends of a scan are significantly different (as can be caused by diffraction maxima from pressure cell components, *e.g.* Fig. 2*b*) then the lower value can be taken as an estimate of the background level under the diffraction profile from the sample crystal.

The peak width parameter depends on both the instrument and the crystal and can normally be expected to show a slight increase with 2θ that can be successfully modelled as a function $\Gamma = a + b \tan \theta$. In order to obtain the parameters a and b the entire data set is integrated, with the parameters Γ, intensity and position refined independently for each reflection, while the background level is determined and fixed for each reflection, and η and I_{ratio} are kept fixed at the predetermined values. The variation of Γ with 2θ is then determined from the refined values for the strong reflections [typically $I > 30$e.s.d.(I), where e.s.d. is the estimated standard deviation or 'standard uncertainty'] that also pass the peak profile tests outlined above and shown in Fig. 1.

The **UB** matrix can also be reliably determined from the setting angles of this same set of strong reflections. The setting angles 2θ, χ and φ at which the data collection scan of each reflection was performed are copied from the input data, and the ω angle assigned to each reflection is the position of the α_1 component of the diffraction peak, as obtained from the least-squares fitting of the diffraction profile. In this way, unit-cell parameters can be obtained that are independent of the range of 2θ values of the reflections used in the refinement (Angel *et al.*, 2000). Refinement of crystal offsets or diffractometer aberrations such as circle zero-errors can be incorporated by the iterative method of Dera & Katrusiak (1999) and symmetry-constrained unit-cell parameters can be obtained by the method of vector-least-squares (Ralph & Finger, 1982).

3.2. Main integration

Once the peak parameters and **UB** matrix have been determined, the integration of the whole data set can be performed by refining only the intensity and position for each profile, and the full set of peak profile tests (Fig. 1) are performed on the results of every reflection. Note that the integrated intensities obtained for the stronger peaks in the pre-processing stage are discarded in order to integrate the entire data set on the same basis. As Pavese & Artioli (1996) demonstrated, this constrained refinement leads to a greater proportion of weak intensities being successfully integrated on a first pass than would be obtained by 'counting' methods of integration. Nonetheless, for weak reflections, or reflections in areas of high and structured background, even the simultaneous refinement of peak position and intensity alone is unstable and often results in negative integrated intensities even though a weak maximum can be present in the scan range.

Although the positions (*i.e.* ω values of the peak maxima) should be described by the **UB** matrix, tests have shown that the calculated position of a peak is often displaced from the observed position in the data collection scan by a few hundredths of a degree. These errors can be attributed to setting-angle errors and other experimental uncertainties. The errors are often smaller if the effects of crystal offsets are included in the calculation of reflection positions, but the offsets are still sufficient to bias the integrated intensity values of strong reflections. Therefore, it is not recommended to use the position calculated from the **UB** matrix in the first attempt at fitting a reflection.

If the profile fails a test, the process of recovery is implemented. The vector $\mathbf{h}_\varphi = \mathbf{UB} \cdot \mathbf{h}$ is calculated (Busing & Levy, 1967) and the value of ω consistent with the values of the components of $\mathbf{h}_\varphi$ and the setting angles 2θ, χ and φ for the reflection is found. If crystal offsets or an ω circle zero were determined along with the refinement of the **UB** matrix, the effect of these is included in the calculation. The peak profile function is then refined again with the ω position of the α_1 peak fixed at this calculated value. After this refinement, the same series of tests are applied to the refined parameters. Profiles that failed a test on the first integration pass because of aberrant peak shape will again fail on this second refinement with constrained peak position. Profiles that are valid but include only weak maxima will, in general, be successfully

integrated. For such weak maxima, a small inaccuracy in calculated peak position does not introduce a significant bias in the integrated intensity because the intrinsic uncertainty in the integrated intensity is relatively large.

3.3. Some observations on statistics

Normally e.s.d.(I) is assigned to reflections on the basis of counting statistics so that one obtains the well known relations:

$$I = P - (n_p/n_b)B,$$
$$\text{e.s.d.}(I) = [P - (n_p/n_b)^2 B]^{1/2}, \quad (3)$$

in which P is the total number of counts in the n_p channels assigned to the peak, and B is the total number of counts in the n_b channels assigned to the background. This is independent of the method by which the peak and background limits are assigned. The e.s.d.(I_{fit}) obtained by least-squares fit of the data with a profile function has a much less direct dependence on the intensity:

Figure 3
A plot of I/e.s.d.(I) for an intensity data set with high signal-to-noise ratio. It was collected from an 'IUCr' ruby sphere with an Xcalibur diffractometer and Mo $K\alpha$ radiation (40 kV, 30 mA) in 'constant precision' mode. Part (b) is an enlargement of the low-intensity region of part (a). Open symbols are estimates of I/e.s.d.(I) obtained by counting integration and a fixed background interval; closed symbols are I_{fit}/e.s.d.(I_{fit}) obtained by integration. The two sets of intensities have been placed on the same numerical scale for ease of comparison. Both methods of integration produce similar results for weak reflections only collected in the prescan, and those collected with the second scan aimed at obtaining I/e.s.d.(I) = 33. Counting methods produce the expected parabolic dependence of I/e.s.d.(I) with intensity for strong reflections only collected with the fast prescan, whereas I_{fit}/e.s.d.(I_{fit}) is approximately constant for these reflections.

$$\text{e.s.d.}(I_{\text{fit}}) \propto V_{II}^{1/2}(\chi_w^2)^{1/2}$$
$$= V_{II}^{1/2}\left[\frac{1}{n-m}\sum_{i=1}^{n}\frac{1}{y_{i,\text{obs}}}(y_{i,\text{obs}} - y_{i,\text{calc}})^2\right]^{1/2}, \quad (4)$$

in which the term V_{II} is the variance of the intensity derived from the least-squares fit of the observed profile represented by the n data points $y_{i,\text{obs}}$ in the profile, $y_{i,\text{calc}}$ are the corresponding calculated values from the refined profile function, and m is the number of refined variables in the profile function.

For the majority of data of intermediate intensities collected on a diffractometer with a rescan so as to attain a specified constant precision in terms of I/e.s.d.(I), the estimates of this ratio are similar for both methods (Fig. 3); for these reflections I/e.s.d.(I) $\simeq I_{\text{fit}}$/e.s.d.(I_{fit}). But for strong reflections in which the background level is insignificant compared with the intensity on the diffraction peak, the two estimates of I/e.s.d.(I) diverge. When $I \gg B$ counting statistics [equation (3)] suggests that I/e.s.d.(I) $= I^{1/2}$. But for the fitting method [equation (4)], both $V_{II}^{1/2}$ and $(\chi_w^2)^{1/2}$ scale approximately with $(I_{\text{fit}})^{1/2}$, so that one obtains the relationship for strong reflections that e.s.d.(I_{fit}) $\propto I_{\text{fit}}$ or that the ratio I_{fit}/e.s.d.(I_{fit}) remains a constant (Fig. 3a).

An assessment of which estimate of e.s.d.(I) is the better estimator of the true uncertainty of the intensity measurements of the stronger reflections can be made by averaging intensity data for a high-symmetry crystal. This allows the comparison of the population standard deviation of symmetry-equivalent intensities with the estimated standard deviations of the individual intensities (*e.g.* Blessing, 1987). For high-quality test crystals, such as the ruby spheres distributed at the Ottawa IUCr congress, it appears that the e.s.d.(I) based on counting statistics significantly overestimates the reproducibility (population standard deviation) of strong
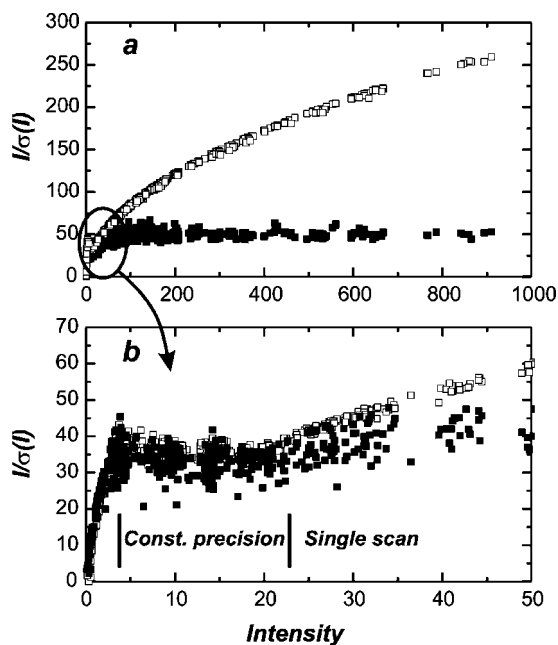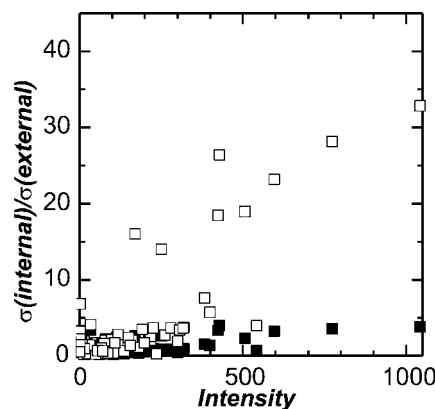

Figure 4
A plot of the ratio of the population standard deviation of symmetry-equivalent reflections, σ_{int}, to σ_{ext} derived from the e.s.d.'s assigned to the individual intensities (after Blessing, 1987) for the two data sets shown in Fig. 3. The large values for the strong reflections with e.s.d.(I) derived from counting (open symbols) compared with those from e.s.d.(I_{fit}) (closed symbols) indicate that the latter is a better estimate of the reproducibility of the measurements of integrated intensities. The result appears to be a general phenomenon for all data sets examined.

reflections, whereas e.s.d.(I_{fit}) from fitting is a better estimate of the true uncertainty of the peak intensity (Fig. 4).

4. Conclusions

Peak profiling methods borrowed from powder diffraction provide a means by which tests for diffraction peak shapes can be defined in a quantitative manner, thereby allowing the automation of the integration of step-scanned intensity data. This has particular merit in those cases where diffraction peaks from the components of environmental cells, such as diamond-anvil cells, interfere with the diffraction data from the sample crystal. As an example consider the profiles shown in Figs. 2(*b*) and 2(*c*). The peak profiling method returns values of the integrated intensities that are in good agreement with those from scans of symmetry-equivalent reflections that are not affected by such interference; the value of the averaged structure factor divided by the population standard deviation, $\bar{F}/\sigma_{int}(\bar{F})$ (after Blessing, 1987), is 37. By contrast, the fixed-background method of integration by counting yields an underestimate of the true intensity for the profile in Fig. 2(*b*), and an overestimate of that in Fig. 2(*c*). The value of $\bar{F}/\sigma_{int}(\bar{F})$ is therefore significantly worse (5.1). In this case, the reflection of Fig. 2(*b*) was then excluded as an outlier (Blessing, 1987). But in cases where symmetry equivalents were not accessible, such an incorrect intensity would not be identified, to the detriment of the structure refinement.

The ideas presented in this paper have been implemented in a software package for Microsoft Windows, *WinIntegrStp*, which is available at http://www.crystal.vt.edu/. The software can handle several input file formats from several commercial diffractometer control packages and accommodates, *via* an editable instrument parameter file, various monochromator and diffraction geometries, including truly monochromatic data from synchrotron sources. The software is fully documented and provides the user with the opportunity to control the testing procedures described in this paper.

Although the procedures for peak integration have been described in the context of step-scanned data collected with a point detector, there is no reason in principle why a similar approach cannot be applied to the integration of data from area detectors. Such an application would require the collection of data in relatively narrow frames so that each profile would appear in several consecutive images. Integration of the individual images would then yield a profile for analysis, although one might wish to combine these two conceptual steps into a single calculation in which an appropriate three-dimensional profile function was fitted directly to the data.

References

Angel, R. J., Downs, R. T. & Finger, L. W. (2000). *High-Pressure and High-Temperature Crystal Chemistry*, *Reviews of Mineralogy and Geochemistry*, Vol. 41, edited by R. M. Hazen & R. T. Downs, pp. 559–596. Washington, DC: MSA.

Blessing, R. (1987). *Crystallogr. Rev.* **1**, 3–58.

Blessing, R., Coppens, P. & Becker, P. (1974). *J. Appl. Cryst.* **7**, 488–492.

Busing, W. & Levy, H. (1967). *Acta Cryst.* **22**, 457–464.

Dera, P. & Katrusiak, A. (1999). *J. Appl. Cryst.* **32**, 510–515.

Destro, R. & Marsh, R. (1987). *Acta Cryst.* **A43**, 711–718.

Diamond, R. (1969). *Acta Cryst.* **A25**, 43–55.

Finger, L. W. & King, H. (1978). *Am. Mineral.* **63**, 337–342.

Gałdecka, E. (1993). *Acta Cryst.* **A49**, 116–126.

Gałdecka, E. (1999). *J. Appl. Cryst.* **32**, 827–832.

Gałdecka, E. (2002). *J. Appl. Cryst.* **35**, 641–643.

Lehmann, M. S. & Larsen, F. K. (1974). *Acta Cryst.* **A30**, 580–584.

Loveday, J. S., McMahon, M. I. & Nelmes, R. J. (1990). *J. Appl. Cryst.* **23**, 392–396.

Pavese, A. & Artioli, G. (1996). *Acta Cryst.* **A52**, 890–897.

Ralph, R. & Finger, L. W. (1982). *J. Appl. Cryst.* **15**, 537–539.